International Journal of Astrobiology 7 (3 & 4): 271–278 (2008) Printed in the United Kingdom
doi:10.1017/S1473550408004291

Oxaloacetate-to-malate conversion by mineral photoelectrochemistry: implications for the viability of the reductive tricarboxylic acid cycle in prebiotic chemistry

Marcelo I. Guzman and Scot T. Martin

School of Engineering and Applied Sciences & Department of Earth and Planetary Sciences, Harvard University, Cambridge, MA 02138, USA
e-mail: scot_martin@harvard.edu

Abstract: The carboxylic acids produced by the reductive tricarboxylic acid (rTCA) cycle are possibly a biosynthetic core of initial life, although several steps such as the reductive kinetics of oxaloacetate (OAA) to malate (MA) are problematic by conventional chemical routes. In this context, we studied the kinetics of this reaction as promoted by ZnS mineral photoelectrochemistry. The quantum efficiency ϕ_{MA} of MA production from the photoelectrochemical reduction of OAA followed $\phi_{MA} = 0.13\,[OAA]\,(2.1 \times 10^{-3} + [OAA])^{-1}$ and was independent of temperature (5 to 50 °C). To evaluate the importance of this forward rate under a prebiotic scenario, we also studied the temperature-dependent rate of the backward thermal decarboxylation of OAA to pyruvate (PA), which followed an Arrhenius behavior as $\log(k_{-2}) = 11.74 - 4956/T$, where k_{-2} is in units of s^{-1}. These measured rates were employed in conjunction with the indirectly estimated carboxylation rate of PA to OAA to assess the possible importance of mineral photoelectrochemistry in the conversion of OAA to MA under several scenarios of prebiotic conditions on early Earth. As an example, our analysis shows that there is 90% efficiency with a forward velocity of 3 yr/cycle for the OAA→MA step of the rTCA cycle at 280 K. Efficiency and velocity both decrease for increasing temperature. These results suggest high viability for mineral photoelectrochemistry as an enzyme-free engine to drive the rTCA cycle through the early aeons of early Earth, at least for the investigated OAA→MA step.

Received 31 July 2008, accepted 5 September 2008

Key words: origin of life, photoelectrochemistry, prebiotic chemistry, reductive citric acid cycle, tricarboxylic acid cycle, zinc sulphide.

Introduction

There are five known mechanisms by which autotrophic organisms fix carbon (Thauer 2007). Of these, however, a reductive tricarboxylic acid (rTCA) cycle, which is alternatively called the reverse Krebs cycle and the reductive citric acid cycle (Scheme 1), has been proposed as the most plausible metabolic pathway of CO_2 fixation at the time life originated (Wachtershauser 1990). That is, the rTCA cycle has been hypothesized as older than the origin of life, implying that it operated under non-enzymatic conditions. A non-enzymatic rTCA cycle might have functioned as an autocatalytic network of chemical reactions able to provide and self-sustain the biosynthetic pathways essential for life to originate (Wachtershauser 1993; Morowitz *et al.* 2000; Smith & Morowitz 2004). In this context, the rTCA cycle has also been suggested as the origin of the catabolic oxidative tricarboxylic acid cycle. The rTCA cycle also supplies metabolites for various biosynthetic pathways. For these reasons, a non-enzymatic rTCA cycle has received much attention in regard to the origin and evolution of life (Aoshima 2007).

The rTCA cycle consists of reduction, carboxylation and dehydration reactions through a linear sequence of 11 carboxylic acids, which overall converts CO_2 to citrate (Scheme 1). Kinetic considerations, however, show important limiting constraints for the viability of this cycle by non-enzymatic pathways (Ross 2007). Specifically, slow reaction rates occur in the linear forward sequence compared with competing side and backward pathways. These unfavourable kinetics are explained at least in part by thermodynamically unfavourable endoergic steps. Recently, however, some of the endoergic reductive steps of the rTCA cycle were demonstrated as feasible through mineral photoelectrochemistry by the semiconductor mineral ZnS (sphalerite or wurtzite) (Zhang &

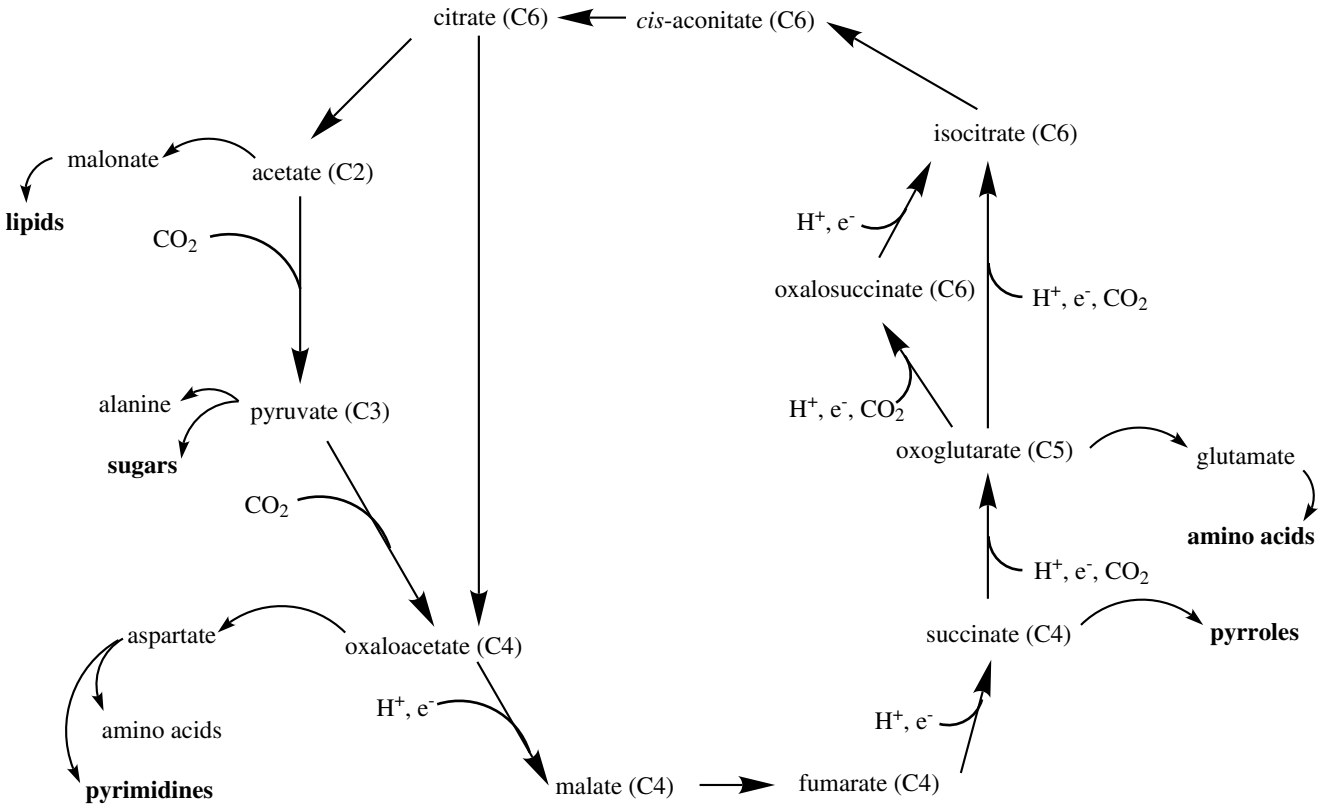

Scheme 1. The reductive tricarboxylic acid cycle as an engine for the synthesis of several major classes of biomolecules. Adapted from Smith & Morowitz (2004).

Martin 2006). During ultraviolet irradiation, conduction band electrons with photoreducing ability are formed (Hoffmann *et al*. 1995).

A critical point needing clarification for these earlier general findings demonstrating feasibility is to establish and constrain whether, for the specific conditions of the prebiotic world, the rTCA cycle can occur and self-sustain at a viable rate (Orgel 2000) when assisted by photoelectrochemistry (Schuster 2000). In this paper, we select one step of the rTCA cycle as a prototypical example and test its viability in detail under relevant prebiotic conditions. Specifically, we consider the viability of the photoelectrochemically driven rTCA reaction oxalosuccinate-to-malate reduction (Scheme 2). We measure the forward rate compared with the reverse oxaloacetate-to-pyruvate decomposition. The analysis supports that the non-enzymatic oxalate-to-malate pathway is viable for a wide range of prebiotic scenarios.

On prebiotic Earth 3.5 to 3.9 Ga ago, the atmospheric composition was dominated by N_2, with important amounts of other gases, including 0.1 to 10 atm CO_2 (Kasting 1993). In the absence of O_3, wavelengths as short as 200 nm reached Earth's surface, penetrating into the oceans. A candidate environment for putting our laboratory study into context can be explored by adapting the conditions of today's hydrothermal sea vents to geochemical conditions in the past. Shallow-water vents are most relevant to photochemistry

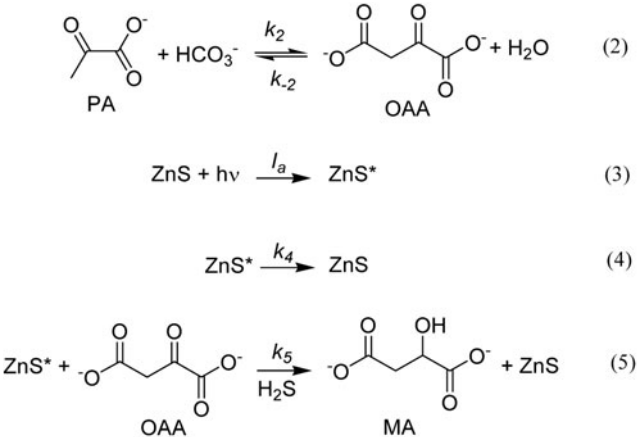

Scheme 2. Reduction of oxaloacetate (OAA) to malate (MA) competing against decarboxylation of OAA to pyruvate (PA). Reaction numbers correspond to those shown in the main text.

because ultraviolet light can penetrate. In these environments, the ocean waters receive warm gaseous and dissolved substances from these vents and exchange gases with the atmosphere. The concentrations of H_2S, H_2 and CH_4 in the venting fluid are in the ranges 0.1–2400, 0.001–0.220, and 0.007–0.200 $\mu M\ kg^{-1}$, respectively (Tarasov *et al.* 2005). Zn(II) concentrations range from 0.1 to $>10\ \mu M$ and can be taken as the expected lower limit for the conditions of early

Earth. Compared with vent fluids of 10 to 120 °C, surrounding waters are between 3 and 30 °C. In prebiotic ocean waters (Holland 1984) between pH 5.5 and 8 (Morse & Mackenzie 1998), high concentrations of aqueous HS^- and Zn^{2+} are expected to have precipitated after cooling as low-solubility ZnS. Widespread occurrence of colloidal ZnS and other semiconducting minerals would have been capable of driving photoelectrochemical reactions in the top 200 m of the prebiotic ocean.

Experimental

Preparation of ZnS colloidal suspensions

A stock solution of 200 mM $ZnSO_4$ (zinc sulphate heptahydrate, EM Science, Germany, 99.5% assay) was employed, together with a saturated stock solution of Na_2S (EMD chemicals, 98% assay) that was kept in an O_2-free environment, to prepare diluted suspensions for irradiation experiments. A suspension of ZnS colloid was prepared at 20 °C by the addition of 240 mL of 52 mM $ZnSO_4$ to 240 mL of nominally 52 mM Na_2S added dropwise while stirring and continuously purging with ultra-high-purity argon gas. Argon-purged ultrapure Millipore water (18.2 MΩ cm) was used. The sulphide concentration in the stock Na_2S solution with 1:100 dilution in 50% sulphide antioxidant buffer (SAOB) was determined by potentiometric titration with a 0.1 M $Cd(NO_3)_2$ standard (cadmium nitrate tetrahydrate, Fluka purum) using a sulphide ion selective electrode (Thermo Electron Corporation, Model Orion 94-16). SAOB was prepared from 80 g NaOH, 35 g ascorbic acid, and 67 g disodium ethylene diamine tetraacetic acid in 1000 mL water. Particle size, surface area, structure, morphology and surface defects of this kind of ZnS particle have been previously characterized (Zhang *et al.* 2007).

Photochemistry experiments

Suspensions for the photochemistry experiments were prepared just prior to use. Oxaloacetic acid (CALBIOCHEM 98%) of 1.5 to 10 mM was added to the ZnS colloid, and the total volume was adjusted to 500 ml by the addition of concentrated H_2SO_4 (EMD Chemicals, 98.0% assay), 1 M NaOH, ultrapure water and Na_2S stock solution. The Na_2S concentration was 8 mM, and the initial pH was 7.0. The excess Na_2S served to scavenge valence-band holes from ZnS during the course of the reaction, as well as to eliminate any adventitious O_2. The colloidal suspension had a loading of 2.3 g L^{-1} ZnS.

The photochemical apparatus (Ace Glass, Vineland, NJ) consisted of a 500 ml glass reaction vessel outfitted with a water jacket to provide a thermostat/cryostat capability (Neslab RTE-111) of between 278 and 323 K. A 450 W medium-pressure ultraviolet mercury arc lamp was inserted in a quartz immersion well in the centre of the reaction vessel. The system was sealed and purged to exclude ambient O_2. The ZnS suspension was constantly stirred during the irradiation. The light intensity between 200 and 400 nm (7.4×10^{-6} Einstein s^{-1}) was measured by actinometry with potassium iron(III) oxalate (Kuhn *et al.* 2004).

Reactant and product analysis

Following irradiation for a selected time period, 1.0 mL of solution was withdrawn from the reaction vessel through a septum and passed through a 0.2 μm syringe filter to prepare for reactant and product analysis (IC Acrodisc 25 mm syringe filters, 0.2 μm pore size; Pall Corporation). The identity and the concentration of carboxylic acids in the filtrate were determined by ion chromatography. A Dionex ICS-3000, equipped with an IonPac AS11-HC analytical column (4 × 250 mm) and an IonPac AG11-HC guard column (4 × 50 mm), was used with conductivity detection and ASRS-ULTRA(II) (4 mm) suppression. A carbonate-free 100 mM NaOH eluent was prepared from a 50.3% sodium hydroxide solution (Fluka puriss) and ultrapure Millipore water (18.2 MΩ cm). A sodium-hydroxide gradient separation was applied, in which the mobile phase began at 2.5 mM NaOH for 2 min and was followed by a linear increase of 3.0 mM min^{-1} up to 54.0 mM NaOH for 5 min. Chemical species were identified by matching the retention times of pure standards. Concentrations were obtained from calibration curves. Standards included oxaloacetic acid ($pK_{a1} = 2.85$, $pK_{a2} = 3.85$), sodium pyruvate (Sigma-Aldrich ReagentPlus 99%), and malate (L-malic acid, disodium salt monohydrate, Sigma Aldrich 98%; $pK_{a1} = 3.46$, $pK_{a2} = 5.10$).

Decarboxylation experiments

Thermal decarboxylation kinetics were measured for the conversion of OAA to PA in the dark for 1.0 mM OAA at an initial pH of 7 and for temperatures in 5 K intervals from 278 to 323 K. OAA solutions were freshly prepared by adding solid oxaloacetic acid to a well-stirred NaOH solution adjusted to pH = 7.0. A complication was that pH rose during the experiment because H^+ was consumed by protonation of the enolate of the pyruvate product. To rule out any change in the rate of thermal decarboxylation over this range of change in pH, we ran analogous experiments in bicine buffer (Alfa Aesar, 99%) at pH = 8.0 and 278, 298 and 318 K. In related experiments, we amended some solutions with variable concentrations of aqueous Zn(II) from $ZnSO_4$.

Results and discussion

The viability of the photoelectrochemically driven OAA to MA reduction of the rTCA cycle can be assessed by an analysis of the reaction kinetics (reactions 2–5 of Scheme 2). The derivation presented in the appendix shows that the efficiency ξ of MA production from OAA relative to PA production from OAA decomposition (i.e., the forward compared with the backward directions of the rTCA cycle) is given by Eq. (1a) (see below). Furthermore, the derivation shows that the half-life $t_{1/2}$ of PA loss towards MA production (i.e., the speed of the forward direction of the rTCA cycle) is expressed in Eq. (1b) for OAA at steady state:

$$\xi = (1 + k_{-2}/\gamma I_a)^{-1} \quad \text{where} \quad \gamma = k_4 k_5^{-1} \tag{1a}$$

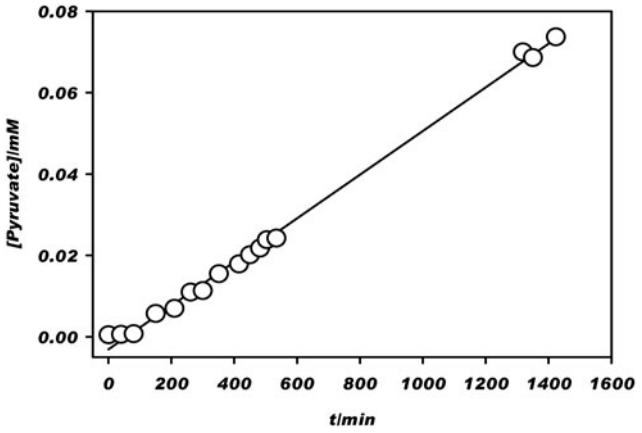

Fig. 1. Kinetics of the thermal decarboxylation of oxaloacetate. Pyruvate is the stochiometric product. The slope of the linear fit yields a rate constant $k_{-2} = 8.9 \times 10^{-7}\ s^{-1}$. Conditions: dark, neat solution (i.e., no colloidal ZnS or added $ZnSO_4(aq)$), 278 K, pH = 7.0, and 1 mM oxaloacetate.

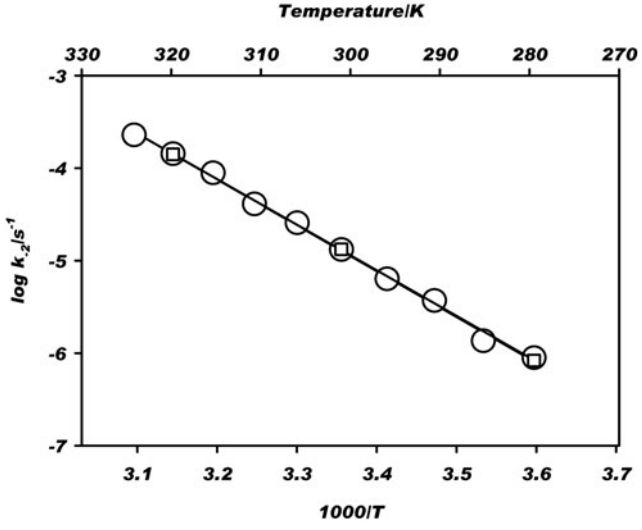

Fig. 2. Temperature dependence of the rate constant k_{-2} for the thermal decarboxylation of oxaloacetate. Circles: initial pH of 7.0. Rectangles: pH = 8.0 in bicine buffer. Other conditions are as indicated for Fig. 1.

$$t_{1/2} = \ln 2/k' \quad \text{where} \quad k' = \frac{K_{2,-2}[HCO_3^-]}{\gamma I_a^{-1} + k_{-2}^{-1}} \tag{1b}$$

In Eqs (1a) and (1b), I_a (Einstein s^{-1}) is the absorbed light intensity, k_i refers to the reactions in Scheme 2, and $K_{2,-2}$ is the equilibrium constant of reaction 2. Among other factors, the half-life through the pseudo-first order rate constant k' depends on temperature via $[HCO_3^-]$, $K_{2,-2}$, and k_{-2}, on light intensity via I_a and k_4, and on catalyst properties via k_4 and k_5. Investigations for k_{-2}, $K_{2,-2}$, and γ are discussed below, while holding constant light intensity and catalyst properties but investigating the dependence on temperature, so that the efficiency and the half-life given by Eqs (1a) and (1b) can be estimated and hence the viability of the rTCA step of OAA→MA by mineral photoelectrochemistry can be assessed for early Earth conditions.

Table 1. *Values of k_{-2}, $K_{2,-2}$, and k' from 273 to 323 K and pH = 7.0*

T (K)	k_{-2} (s^{-1})	$K_{2,-2}$ (M^{-1})	k' (s^{-1})
273	4.0×10^{-7}	6.0×10^{0}	1.4×10^{-7}
278	8.5×10^{-7}	4.3×10^{-1}	1.8×10^{-8}
283	1.8×10^{-6}	3.4×10^{-2}	2.6×10^{-9}
288	3.5×10^{-6}	3.0×10^{-3}	3.9×10^{-10}
293	6.9×10^{-6}	2.8×10^{-4}	6.3×10^{-11}
298	1.3×10^{-5}	2.8×10^{-5}	1.1×10^{-11}
303	2.5×10^{-5}	3.1×10^{-6}	2.0×10^{-12}
308	4.6×10^{-5}	3.7×10^{-7}	3.8×10^{-13}
313	8.4×10^{-5}	4.6×10^{-8}	7.7×10^{-14}
318	1.5×10^{-4}	6.2×10^{-9}	1.6×10^{-14}
323	2.6×10^{-4}	9.0×10^{-10}	3.7×10^{-15}

Oxaloacetate decarboxylation: k_{-2}

Figure 1 shows the concentration of PA for increasing time at 5 °C and pH = 7.0, from which the rate constant k_{-2} for the thermal decarboxylation of OAA is obtained. The forward and backward reactions are as follows (Scheme 2):

$$\text{pyruvate}^- + HCO_3^- \underset{k_{-2}}{\overset{k_2}{\rightleftharpoons}} \text{oxaloacetate}^{2-} + H_2O. \tag{2, -2}$$

From 5 to 50 °C, the measured rate constants are plotted as $1/T$ in Fig. 2. Results are shown both for a buffer medium of bicine at pH = 8.0 as well for unbuffered solution initially at pH = 7.0, demonstrating a negligible effect of pH over this range. The pH increases from 7.0 during the course of an unbuffered experiment because of HCO_3^- production. The relationship k_{-2} versus $1/T$ has an Arrhenius dependence as $\log(k_{-2}) = 11.74 - 4956/T$, where k_{-2} is in units of s^{-1}, with an apparent activation energy $E_{a,-2}$ of 94.6 kJ mol^{-1} and an A-prefactor of $4.9 \times 10^{11}\ s^{-1}$. The values of these parameters are consistent with those of other β-oxocarboxylic acids (Gelles 1956; Guthrie 2002).

Pyruvate carboxylation: $K_{2,-2}$

The free energy of reaction $\Delta_r G^\circ$ for equilibrium (2, −2) is 25.94 kJ mol^{-1} at 298 K, corresponding to $K_{2,-2} = 2.837 \times 10^{-5}\ M^{-1}$ (Wood *et al.* 1966; Miller & Smith-Magowan 1990). The values of $K_{2,-2}$ at other temperatures, obtained from the integrated van't Hoff equation, are presented in Table 1. This equation is given by

$$K_{2,-2}(T_2) = K_{2,-2}(T_1)\exp\left[-(\Delta_r H^\circ/R)(1/T_2 - 1/T_1)\right]$$

and requires for evaluation the reaction enthalpy. The reaction enthalpy for pyruvate carboxylation $\Delta_r H^\circ(2, -2)$ can be obtained from the standard enthalpies of formation $\Delta_f H^\circ$ (aq) of the reactants and products in aqueous solution for standard states of 1 M for the ions and unit activity for water (i.e. pure water) (Miller & Smith-Magowan 1990; Kishore *et al.* 1998):

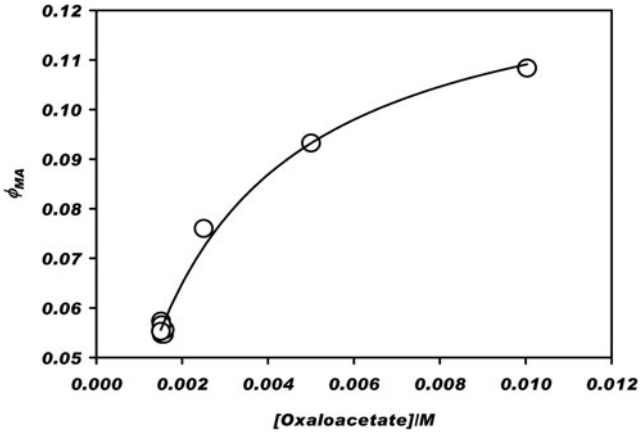

Fig. 3. Quantum efficiency ϕ_{MA} for the photoelectrochemical production of malate (MA) from several concentrations of oxaloacetate (OAA). The fitted curve yields $\phi_{MA} = 0.13$ [OAA] $(2.1 \times 10^{-3} + [OAA])^{-1}$. Conditions: 2.3 g l^{-1} ZnS mineral, HS^- valence band hole scavenger, pH = 7.0, irradiated at $\lambda > 200$ nm, 293 K, and pH = 7.0. Control experiments: no malate was detected in the absence of any one of UV light, ZnS catalyst, H_2S hole scavenger, or oxaloacetate reactant.

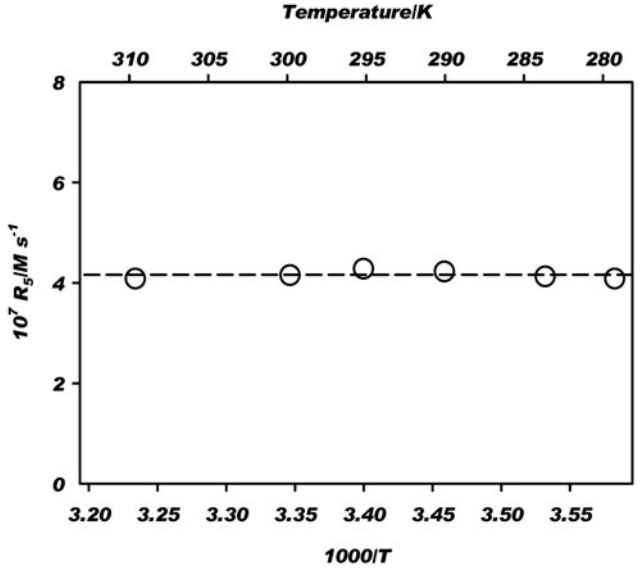

Fig. 4. Temperature independence of the photoelectrochemical production rate of malate from oxaloacetate. The horizontal line shows the mean production rate of 4.2×10^{-7} M s^{-1}. Conditions: as indicated for Fig. 3 for 1.5 mM oxaloacetate.

$$\underset{-591.57}{\text{Pyruvate}^-(aq)} + \underset{-698.93}{\text{HCO}_3^-(aq)} \underset{k_{-2}}{\overset{k_2}{\rightleftarrows}} \underset{-672.90}{\text{oxaloacetate}^{2-}(aq)} + \underset{-285.00}{\text{H}_2\text{O}} \qquad (2, -2)$$

$\Delta_f H^\circ(aq)$ (kJ mol^{-1}):

Then, $\Delta_r H^\circ(2, -2) = 331.74$ kJ mol^{-1}. For comparison with $\Delta_r G^\circ(2, -2) = 25.94$ kJ mol^{-1} at 298 K, Smith & Morowitz (2004) reported 62.1 kJ mol^{-1}, but this value appears incorrect; which can be explained by the omission of the water molecule in their calculation.

Oxaloacetate-to-malate photoreduction: γ

Figure 3 shows the quantum efficiency ϕ_{MA} of MA production from OAA in the presence of ZnS colloid for several concentrations of OAA. The mechanism of photoelectrochemistry can be simplified into photoexcitation, charge–carrier recombination, and reductive chemistry, as represented by reactions 3 to 5:

$$\text{ZnS} + h\nu \overset{I_a}{\rightarrow} \text{ZnS}^* \qquad (3)$$

$$\text{ZnS}^* \overset{k_4}{\rightarrow} \text{ZnS} \qquad (4)$$

$$\text{ZnS}^* + \text{OAA}^{2-} \underset{\text{H}_2\text{S}}{\overset{k_5}{\rightarrow}} \text{MA}^{2-} + \text{ZnS} \qquad (5)$$

where ZnS* indicates an excited state. ZnS* can undergo relaxation through electron-hole pair recombination (reaction 4) or alternatively reduce OAA to produce MA (reaction 5) using a conduction band electron e^-. The hole scavenger in this case is HS^-. The composite rate coefficient j_5 of MA photoproduction, which is equal to that of OAA loss by Eq. (5), can be expressed as $d[MA]/dt = -d[OAA]/dt = j_{(5)}$ $[OAA] = k_5$ [ZnS*] [OAA], implying that $j_5 = k_5[ZnS^*]$, where j_5 (s^{-1}) $\equiv \phi_{MA} I_a/[OAA]$ and ϕ_{MA} is the quantum yield. From Eqs (3)–(5), we write at steady state (see the Appendix) that $[ZnS^*] = I_a(k_4 + k_5\ [OAA])^{-1}$, implying that $\phi_{MA} = [OAA]$ $(\gamma + [OAA])^{-1}$. The data of Fig. 3 fit this model for $\gamma = k_4/k_5 = 2.1 \times 10^{-3}$ M, which is shown as the solid line in the figure. Quantum yield is expected to depend on light intensity, colloidal particle surface area, pH, surface and bulk structures and defects, among other factors, all of which are held constant in this study, allowing the lumping of these terms into an effective coefficient j_5. In our analysis, we assume that these factors regarding catalyst properties in our laboratory study are representative of the photoelectrochemical properties of ZnS colloidal particles in the oceans of early Earth.

Figure 4 shows that the photoelectrochemical production rate of MA is independent of temperature, at least for the range of conditions investigated. Photoelectrochemical reaction rates in the condensed phase are often temperature-independent. There is thus a basic difference in the temperature dependence of the side or back thermal reactions compared with the forward photoreactions, and this difference is important when considering the viability of the forward pathway in the rTCA cycle.

Viability: ξ and $t_{1/2}$

Table 1 and Fig. 5 respectively show k_{-2}, $K_{2,-2}$, and k' and the evaluation of ξ and $t_{1/2}$ as a function of temperature. For the calculation of k', an expression for the dependence of $[CO_2(aq)]$ (M) on temperature at 1 atm CO_2 was used (Lide 2008):

$$[\text{CO}_2(aq)] = 10^{(997.38/T - 4.8011)}. \qquad (6)$$

$[HCO_3^-]$ was obtained as 0.82 $[CO_2(aq)]$ to account for speciation at pH = 7.0. Regarding I_a, the ultraviolet fluxes for 3.5 to 3.9 Ga ago in UVA (315–400 nm), UVB (280–315 nm),

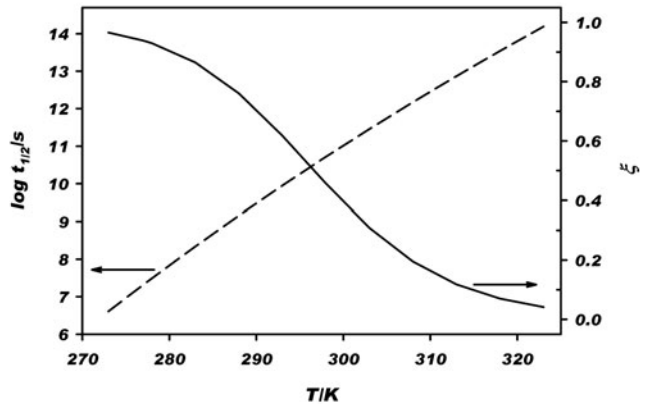

Fig. 5. Temperature dependence of (solid line) the efficiency ξ and (dashed line) the half-life $t_{1/2}$, corresponding to Eqs (1a) and (1b) in the text.

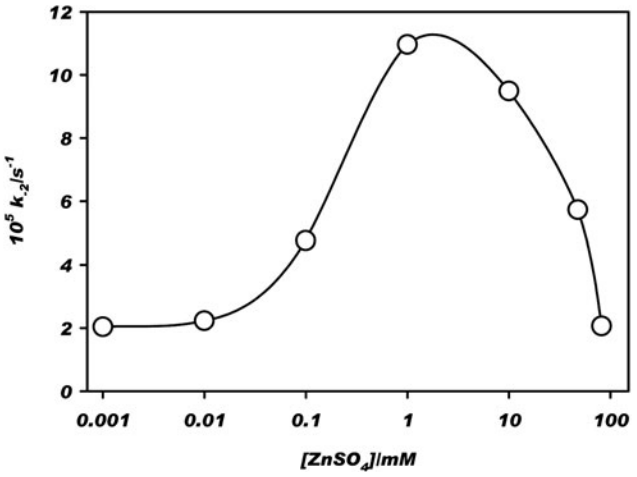

Fig. 6. Effect of aqueous Zn(II) concentration on the rate constant k_{-2} for the thermal decarboxylation of oxaloacetate to pyruvate at 298 K. Other conditions are as indicated for Fig. 1.

and UVC (200–280 nm) were taken as 40, 5, and 1 W m^{-2}, respectively (Cockell 2000), corresponding to a mean total ultraviolet intensity for the prebiotic Earth of 5.5×10^{-3} Einstein s^{-1}. We assume that the ZnS loading was high enough to absorb all of these photons and we omit the screening effects of other chromophores in the ocean waters.

Figure 5 shows that the efficiency ξ of OAA→MA compared with OAA→PA drops from 90% at 280 K to 10% at 314 K, suggesting an increasing viability at lower temperatures. For increasing temperatures the backward thermal decomposition is progressively favored over the forward photoelectrochemical pathway. Over the same temperature range, the half-life of PA conversion towards MA increases from 3 yr at 280 K to 4×10^5 yr at 314 K. For increasing temperature, the forward direction of this step of the rTCA slows, which can be explained by the decreasing efficiency. This study's measurements and the associated analysis presented herein for early Earth conditions therefore support a more efficient and more rapid turning of the rTCA cycle with regard to the OAA→MA step for decreasing temperatures. As an example, at 280 K there is 90% efficiency and 3 yr/cycle forward velocity for the OAA→MA step. These results suggest high viability for mineral photoelectrochemistry as an engine to drive the rTCA cycle through the early aeons of early Earth, at least for the investigated OAA→MA step.

Other factors

In the oceans of early Earth, besides ZnS colloidal particles, aqueous Zn(II) ions are also believed to have been present. A solution of OAA at pH = 7.0 is speciated by more than 99.9% as the dianion and contains the keto:enol:hydrate forms in the ratios 81:12:7, respectively (Pogson & Wolfe 1972; Kokesh 1976; Emly & Leussing 1981). Aqueous Zn(II) can form complexes with the keto and enol structures (Gelles & Hay 1958; Gelles & Salama 1958a,b; Covey & Leussing 1974), and these complexes can promote decarboxylation to form PA. However, further enolization into stable intermediates, such as a dinuclear metal complex species, that hinder decarboxylation is also possible. These pathways could affect the viability of the overall PA→OA→MA sequence, and they should also therefore be considered.

Previous studies of the effect of Zn(II) on decarboxylation rates of OAA have been done at 303 K and pH = 5 and found that for 0.1–32 mM Zn(II), k_{-2} increases by between 10 and 80 times relative to the uncatalysed reaction (Speck 1949). At this pH, speciation is 7% as the monoanion species of OAA ($OAAH^-$), which decarboxylates four times faster than the dianion OAA (OAA^{2-}) (Pedersen 1952). These studies, however, were not carried out for the pH conditions of our study, and the range of Zn(II) concentrations was limited.

We carried out a series of experiments on the possible influence of dissolved Zn(II) on the thermal decomposition of OAA for the range of our experimental conditions. Figure 6 shows the effect of Zn(II) concentration on the decarboxylation rate constant of OAA (k_{-2}) at pH = 7.0 and 298 K. For [Zn(II)] < 0.01 mM, k_{-2} is the same within experimental uncertainty as measured for the unaugmented solution (Table 1). For 0.01 < [Zn(II)] < 1 mM, k_{-2} increases, which can be explained by the formation of reactive keto complexes. The maximum increase is 10-fold. For [Zn(II)] > 1 mM, k_{-2} drops to the unaugmented value. This inhibition results from the formation of unreactive dinuclear enolate metal ion complexes (Covey & Leussing 1974; Tsai & Leussing 1987). The results shown in Fig. 6 bracket the expected range of dissolved Zn(II) in the oceans of early Earth. The values in Fig. 6 are slow enough that they do not influence our conclusions regarding the viability of the oxalate-to-malate transformation by mineral photoelectrochemistry.

Conclusions

The kinetic measurements of this study demonstrate the viability of driving one part of the rTCA cycle (specifically, OAA to MA conversion) by colloidal photoelectrochemistry. They also support the possibility of driving the sequence PA→OAA→MA. These reactions harvest light as the

primordial source of energy and provide a plausible mechanism for the formation of simple, biologically important molecules on early Earth. As an example, our analysis shows that there is 90% efficiency and a forward velocity of 3 yr/cycle for the OAA→MA step of the rTCA cycle at 280 K. Efficiency and velocity both decrease for increasing temperature. On this basis, an enzyme-free conversion OAA→MA on early Earth would have been possible in the rTCA cycle. More generally, the rTCA cycle has four other reductive steps in addition to the selected prototypical reaction OAA→MA (cf. Scheme 1). The viability of each of these other steps can be evaluated on the same basis as presented herein for OAA→MA.

In summary, it is possible that colloidal photoelectrochemistry had an active role on early Earth for converting and cycling small organic compounds essential for the origin of life (Zhang *et al.* 2004, 2007; Zhang & Martin 2006). The interaction of excited-state species and radicals, driven by energy harvested from sun's photons, can open reaction pathways that can be slow by thermal chemistry alone. Reduction reactions can aid in the assembly of some of the building blocks essential to the prebiotic synthesis of even more organized molecules and structures, such as catalysts and bilayers.

Acknowledgments

M.I.G. is the recipient of a Postdoctoral Fellowship from the Harvard Origins of Life Initiative. This study is supported by the National Aeronautics and Space Administration under Grant NNX07AU97G issued through the Office of Space Science.

Supporting information available

Text: calculation of the concentration of $CO_2(aq)$ as a function of temperature in reference to Eq. (6).

Appendix

The rate equation for photoexcited ZnS* follows from reactions 3 to 5:

$$\frac{\mathrm{d}[\mathrm{ZnS}^*]}{\mathrm{d}t} = I_\mathrm{a} - k_4[\mathrm{ZnS}^*] - k_5[\mathrm{ZnS}^*][\mathrm{OAA}]. \tag{A1}$$

Under continuous irradiation, the steady-state approximation for ZnS* allows Eq. (A1) to be written as follows:

$$[\mathrm{ZnS}^*] = \frac{I_\mathrm{a}}{k_4 + k_5[\mathrm{OAA}]}. \tag{A2}$$

The rate of MA production and OAA loss in reaction 5 is given by the following equation:

$$\begin{aligned}\frac{\mathrm{d}[\mathrm{MA}]}{\mathrm{d}t} &= -\left(\frac{\mathrm{d}[\mathrm{OAA}]}{\mathrm{d}t}\right)_{\mathrm{rxn}\ 5} = k_5[\mathrm{ZnS}^*][\mathrm{OAA}] \\ &= \frac{I_\mathrm{a}[\mathrm{OAA}]}{k_4 k_5^{-1} + [\mathrm{OAA}]}.\end{aligned} \tag{A3}$$

For small [OAA], we obtain for reaction 5:

$$\frac{\mathrm{d}[\mathrm{MA}]}{\mathrm{d}t} = -\left(\frac{\mathrm{d}[\mathrm{OAA}]}{\mathrm{d}t}\right)_{\mathrm{rxn}\ 5} = \frac{k_5}{k_4} I_\mathrm{a}[\mathrm{OAA}]. \tag{A4}$$

Using the steady-state approximation for [OAA], we can write for the sum of sources and sinks of OAA:

$$\begin{aligned}\frac{\mathrm{d}[\mathrm{OAA}]}{\mathrm{d}t} &= \left(k_2[\mathrm{PA}][\mathrm{HCO_3^-}]\right)_{\mathrm{rxn}\ 2} - \left(k_{-2}[\mathrm{OAA}]\right)_{\mathrm{rxn}-2} \\ &\quad - \left(\frac{k_5}{k_4} I_\mathrm{a}[\mathrm{OAA}]\right)_{\mathrm{rxn}\ 5} = 0.\end{aligned} \tag{A5}$$

From Eq. (A5), the efficiency ξ of MA production from OAA relative to PA production from OAA decomposition is as follows:

$$\begin{aligned}\xi &= \frac{\left(\frac{k_5}{k_4} I_\mathrm{a}[\mathrm{OAA}]\right)_{\mathrm{rxn}\ 5}}{\left(k_{-2}[\mathrm{OAA}]\right)_{\mathrm{rxn}-2} + \left(\frac{k_5}{k_4} I_\mathrm{a}[\mathrm{OAA}]\right)_{\mathrm{rxn}\ 5}} \\ &= (1 + k_{-2}/\gamma I_\mathrm{a})^{-1}\end{aligned} \tag{1a}$$

where $\gamma = k_4 k_5^{-1}$. From Eqs (A4) and (A5), the overall rate for MA production from PA via OAA is as follows:

$$\frac{\mathrm{d}[\mathrm{MA}]}{\mathrm{d}t} = \frac{K_{2,-2}[\mathrm{HCO_3^-}]}{\gamma I_\mathrm{a}^{-1} + k_{-2}^{-1}}[\mathrm{PA}] \tag{A6}$$

where $K_{2,-2} = k_2/k_{-2}$ for equilibrium PA⇄OAA. For OAA at steady state, the half-life of PA loss towards MA production is expressed in Eq. (1b):

$$t_{1/2} = \ln 2/k' \quad \text{where} \quad k' = \frac{K_{2,-2}[\mathrm{HCO_3^-}]}{\gamma I_\mathrm{a}^{-1} + k_{-2}^{-1}} \tag{1b}$$

References

Aoshima, M. (2007). *Appl. Microbiol. Biotechnol.* **75**, 249–255.
Cockell, C.S. (2000). *Planet. Space Sci.* **48**, 203–214.
Covey, W.D. & Leussing, D.L. (1974). *J. Am. Chem. Soc.* **96**, 3860–3866.
Emly, E. & Leussing, D.L. (1981). *J. Am. Chem. Soc.* **103**, 628–634.
Gelles, E. (1956). *J. Chem. Soc.*, 4736–4739.
Gelles, E. & Hay, R.W. (1958) *J. Chem. Soc.*, 3673–3683.
Gelles, E. & Salama, A. (1958a). *J. Chem. Soc.*, 3683–3688.
Gelles, E. & Salama, A. (1958b). *J. Chem. Soc.*, 3689–3693.
Guthrie, J.P. (2002). *Bioorganic Chem.* **30**, 32–52.
Hoffmann, M.R., Martin, S.T., Choi, W. & Bahnemann, D.W. (1995). *Chem. Rev.* **95**, 69–96.
Holland, H.D. (1984). *The Chemical Evolution of the Atmosphere and Oceans*, pp. 105–107. Princeton University Press, Princeton, NJ.
Kasting, J.F. (1993). *Science* **259**, 920–926.
Kishore, N., Tewari, Y.B. & Goldberg, R.N. (1998). *J. Chem. Thermodynam.* **30**, 1373–1384.
Kokesh, F.C. (1976). *J. Org. Chem.* **41**, 3593–3599.
Kuhn, H.J., Braslavsky, S.E. & Schmidt, R. (2004). *Pure Appl. Chem.* **76**, 2105–2146.
Lide, D.R. (2008). Solubility of carbon dioxide in water at various temperatures and pressures. In *CRC Handbook of Chemistry and Physics*, 88th edn, pp. 8–84. CRC Press/Taylor and Francis, Boca Raton, Fl, USA.
Miller, S.L. & Smith-Magowan, D. (1990). *J. Phys. Chem. Ref. Data* **19**, 1049–1073.
Morowitz, H.J., Kostelnik, J.D., Yang, J. & Cody, G.D. (2000) *Proc. Natl Acad. Sci. USA* **97**, 7704–7708.

Morse, J.W. & Mackenzie, F.T. (1998). *Aquat. Geochem.* **4**, 301–319.
Orgel, L.E. (2000). *Proc. Natl Acad. Sci. USA* **97**, 12 503–12 507.
Pedersen, K.J. (1952). *Acta Chem. Scand.* **6**, 285–303.
Pogson, C.I. & Wolfe, R.G. (1972). *Biochem. Biophys. Res. Commun.* **46**, 1048.
Ross, D.S. (2007). *Orig. Life Evol. Biosph.* **37**, 61–65.
Schuster, P. (2000). *PNAS,* 97, pp. 7678–7680.
Smith, E. & Morowitz, H.J. (2004). *Proc. Natl Acad. Sci. USA* **101**, 13 168–13 173.
Speck, J.F. (1949). *J. Biolog. Chem.* **178**, 315–324.
Tarasov, V.G., Gebruk, A.V., Mironov, A.N. & Moskalev, L.I. (2005). *Chem. Geol.* **224**, 5–39.
Thauer, R.K. (2007). *Science* **318**, 1732–1733.
Tsai, S.J. & Leussing, D.L. (1987). *Inorg. Chem.* **26**, 2620–2629.
Wachtershauser, G. (1990). *Proc. Natl Acad. Sci. USA* **87**, 200–204.
Wachtershauser, G. (1993). *Pure Appl. Chem.* **65**, 1343–1348.
Wood, H.G., Davis, J.J. & Lochmuller, H. (1966). *J. Biol. Chem.* **241**, 5692–5704.
Zhang, X.V., Ellery, S.P., Friend, C.M., Holland, H.D., Michel, F.M., Schoonen, M.A.A. & Martin, S.T. (2007). *J. Photochem. Photobiol. A: Chem.* **185**, 301–311.
Zhang, X.V. & Martin, S.T. (2006). *J. Am. Chem. Soc.* **128**, 16 032–16 033.
Zhang, X.V., Martin, S.T., Friend, C.M., Schoonen, M.A.A. & Holland, H.D. (2004). *J. Am. Chem. Soc.* **126**, 11 247–11 253.

SUPPORTING INFORMATION

Oxaloacetate-to-Malate Conversion by Mineral Photoelectrochemistry: Implications for the Viability of the Reductive Tricarboxylic Acid Cycle in Prebiotic Chemistry

Marcelo I. Guzman and Scot T. Martin

Calculation of $CO_2(aq)$ Concentration as a Function of Temperature

The following procedure was used to obtain the $CO_2(aq)$ concentrations as a function of temperature for the interval 0–50 °C. The CO_2 mole fraction, x_{CO_2}, in liquid phase at pressure $P = 1$ atm $= 101.325$ kPa as a function of temperature, T, was obtained by extrapolation of every pressure P vs. x_{CO_2} data series, at each temperature. Data used for this purpose is in Table 8-84 of the CRC Handbook of Chemistry and Physics (Lide, 2008). In this way a linear fitting is obtained at each temperature:

$$1000\ x_{CO_2} = b_1\ P + b_2 \tag{S1}$$

where P is given in kPa units and b_1 and b_2 represent the slope and intercept coefficients, respectively. Table S1 gathers the linear regression fitting parameters for Equation S1 at $P = 101.325$ kPa as a function of temperature.

Table S1 also shows the conversion of extrapolated x_{CO_2} data at 101.325 kPa to $[CO_2(aq)]$ in molar concentration, results that represent the solubility of CO_2 at variable temperatures. From a linear fitting for the $\log[CO_2(aq)]$ vs. $1/T$ data of Table S1, the following expression to calculate molar $CO_2(aq)$ concentrations as a function of temperature at $P_{CO_2} = 1$ atm is obtained:

$$[CO_2(aq)]/\mathrm{M} = 10^{(997.38/T - 4.8011)} \tag{S2}$$

Table S1. *Linear coefficients for the CO_2 mole fraction dependence with pressure, extrapolated CO_2 mole fraction to 101.325 kPa, and calculated CO_2(aq) molar concentration in water, at variable temperature*

t/°C	T/K	$1000/T$	$10^2\ b_1$	$10^3\ b_2$	$10^3\ x_{CO_2}$	$[CO_2(aq)]$/M
0	273.14	3.661	1.336	1.890	1.3556	0.0712
5	278.14	3.595	1.123	1.070	1.1389	0.0612
10	283.14	3.532	0.9494	1.431	0.9634	0.0529
15	288.14	3.471	0.8137	1.005	0.8255	0.0459
20	293.14	3.411	0.7040	0.5395	0.7139	0.0401
25	298.14	3.354	0.6138	0.7027	0.6226	0.0351
30	303.14	3.299	0.5410	0.4983	0.5487	0.0309
35	308.14	3.245	0.4811	0.4399	0.4879	0.0274
40	313.14	3.193	0.4307	0.5395	0.4369	0.0243
45	318.24	3.143	0.3889	0.4553	0.3945	0.0216
50	323.14	3.095	0.3537	0.5808	0.3590	0.0194

Reference

Lide, D.R. (2008). Solubility of carbon dioxide in water at various temperatures and pressures. In *CRC Handbook of Chemistry and Physics*, 88th edn, 8–84. CRC Press/Taylor and Francis.